

# Optical spectral index - luminosity relation for the 17 mapped Palomar-Green quasars

Xue-Guang Zhang<sup>1,2\*</sup>

<sup>1</sup>*Purple Mountain Observatory, Chinese Academy of Sciences, 2 Beijing XiLu, NanJing, JiangSu, 210008, People's Republic of China*

<sup>2</sup>*Chinese Center for Antarctic Astronomy, NanJing, JiangSu, 210008, People's Republic of China*

## ABSTRACT

In this paper, the optical spectra index - luminosity relationship is checked for the well-known 17 individual mapped QSOs, in order to give one more clearer conclusion on the so far conflicting dependence of the spectral index on the luminosity for AGN. Different from the global relationships based on the color difference (photometry parameters) for samples of AGN, the more reliable relationship is determined for the multi-epoch observed individual mapped QSOs with no contamination from the host galaxies, the line variabilities and the much different central properties. The final confirmed results are as follows. (1): No strong dependence of the optical spectral index on the continuum luminosity can be found for all the 17 QSOs, besides two objects (PG 0026 and PG 1613) having some weak trends (with  $3\sigma$  confidence level) for the relationship. In other words, the common sense 'AGNs get bluer when they get brighter' is not so common. (2): There are much different damped intrinsic variability time scales for the variability modes of the optical spectral index and the continuum emission, through the well applied Damped Random Walk method for the AGN variability. In other words, there are some different intrinsic mechanisms controlling the variabilities of the optical spectral index and the power law AGN continuum emission. Therefore, the much weak dependence of the optical spectral index on the continuum luminosity can be further confirmed.

**Key words:** Galaxies:Active – Galaxies:nuclei – Galaxies:emission lines

## 1 INTRODUCTION

Variability is one of the fundamental characters of Active Galactic Nuclei (AGN) (Ulrich et al. 1997), and moreover, AGN variability is one powerful tool for understanding the structures of the central regions of AGN (Rees 1984, Hawkins 1996, Kawaguchi et al. 1998, Torricelli-Ciamponi et al. 2000, Hawkins 2002, Peterson et al. 2004, Hopkins et al. 2006, Kelly et al. 2009, Breedt et al. 2010, Schmidt et al. 2010, Mushotzky et al. 2011, Zhang 2011, Zu et al. 2011, Zhang 2013a, 2013b, Zu et al. 2013). However, there is so far no clear conclusion about the nature of the AGN variability, besides several well-known dependence of the AGN variability on the other AGN parameters (such as the luminosity, accretion rate, black hole mass, redshift etc., Vanden Berk et al. 2004, Wold et al. 2007, Wilhite et al. 2008). Among the dependence, the dependence of the spectral index (in the paper, we mainly consider the continuum slope  $\alpha$ ,  $f_\lambda \propto \lambda^\alpha$ ) on the AGN luminosity (the spectral index - luminosity relation) is the widely and commonly studied one, since the dependence was found for 3CR extragalactic

galaxies (Heeschen 1960, Conway et al. 1963, Kellermann et al. 1969, Macleod & Doherty 1972). However, the conclusion about the dependence is still uncertain.

In the previous studies, the spectral index - luminosity relationship was commonly checked by samples of AGNs with different redshifts, different luminosities, different black hole masses, different accretion rates, different contamination sources etc.. Therefore, there are so far contradictory statements about the relationship. More recently, Schmidt et al. (2012) have reported that AGN color variability (spectral index) is remarkably uniform, and independent not only of redshift, but also of quasar luminosity and black hole mass, after the correction of the effects from the emission lines in the different SDSS (Sloan Digital Sky Survey) bands, by the sample of 9093 QSOs in the SDSS stripe82. Zuo et al. (2012) have reported that AGN variability increases as either luminosity or Eddington ratio decreases, however, the relationship between variability and black hole mass is uncertain, by 7658 QSOs from SDSS Stripe 82. Certainly, some different results about the spectral index - luminosity relationship can be still found in the literature. Sakata et al. (2010) have shown that the spectral shape of AGN continuum emission in the optical region does not systemati-

\* xgzhang@pmo.ac.cn

cally change during flux variation by the study of 11 nearby Seyfert galaxies. Woo et al. (2007) have shown that after the corrections of the host galaxy light dilutions, the nuclear variability with the similar amplitudes in the g and r bands within the errors, by the study of 13 moderate luminosity AGNs at  $z = 0.36$ . The similar results can be found in Walsh et al. (2009): there are no significant color variations for the 13 nearby AGNs. Meanwhile, we (Zhang et al. 2008) have shown that there is one strong correlation between the spectral index and the dimensionless Eddington accretion rate by 193 broad line AGN with high quality SDSS spectra. Pu et al. (2006) have reported that there was strong global correlation between the spectral index and the continuum luminosity for the QSOs in Kaspi et al. (2000). Wilhite et al. (2005) have reported the clear dependence of the spectral variability on the wavelength by one sample of about 300 variable QSOs with multi-epoch SDSS spectra. Therefore, there is so far no one confirmed conclusion about the spectral index - luminosity relationship.

It is clear that the previous study of the color variability (spectral index) was mainly based on photometry parameters of samples of AGN. Thus, there are apparent effects on the spectral index - luminosity relation from the contributions of the host galaxies and the emission lines, and from the different AGN properties (different BH masses, redshift, accretion rate, etc) of the sample objects. Even though, some effects above can be statistically corrected as discussed in the corresponding literatures, the sample size should have apparent effects on the final conclusion about the spectral index - luminosity relationship (Tang et al. 2007). Therefore it is necessary and interesting to re-check the spectral index - luminosity relationship by the spectroscopic data of the well-known mapped objects. The advantages of using the spectroscopic parameters of the mapped objects are as follows. On the one hand, the effects of the different black hole masses can be totally ignored. On the other hand, the effects of the emission lines can be clearly ignored. Moreover, in the paper, we mainly consider the 17 well known mapped Palomar-Green QSOs (PG QSOs), thus, the effects of the host galaxies can be totally ignored.

The paper is organized as follows. In section 2, we present our method to determine the spectral index of the mapped PG QSOs. Section 3 gives the spectral index - luminosity relationships for the mapped objects. Finally the discussions and conclusions are given in Section 4. In this paper, the cosmological parameters  $H_0 = 70 \text{ km} \cdot \text{s}^{-1} \text{ Mpc}^{-1}$ ,  $\Omega_\Lambda = 0.7$  and  $\Omega_m = 0.3$  have been adopted.

## 2 THE SPECTRAL INDICES OF THE 17 PG QSOs

In order to totally ignore the effects of the host galaxies and/or the probable effects of the flux calibration, the 17 nearby PG QSOs with public spectra (Kaspi et al. 2000) are mainly considered, among all the reported mapped AGN (kaspi et al. 1996, 2000, Peterson et al. 2004, Kaspi et al. 2005, Bentz et al. 2006, Denney et al. 2006, Bentz et al. 2009, Denney et al. 2009, Bentz et al. 2010, Denney et al. 2010, Barth et al. 2011). The detailed description of the 17 PG QSOs can be found in Kaspi et al. (2000). Their spectra were observed using the Steward Observatory 2.3 m

telescope and the Wise Observatory (WO) 1 m telescope for around 7.5 years. Each QSO has more than 20 spectroscopic data points, which lead us to find the more reliable spectra index - luminosity relationship for the 17 individual objects without the global effects. The public spectra have been collected from the website: <http://wise-obs.tau.ac.il/shai/PG/>. Moreover, the spectra have been binned into  $1\text{\AA}$  per pixel and are padded from  $3000\text{\AA}$  to  $9000\text{\AA}$ . Certainly, in most cases the usable part of the spectrum is the blue part around the  $H\beta$  (Maoz et al. 1994, Kaspi et al. 2000). Therefore, in this paper, the spectra around the  $H\beta$  are mainly considered.

Then, based on the multi-epoch observed spectra of the 17 mapped PG QSOs, the spectral index in the optical band (from  $4400\text{\AA}$  to  $5500\text{\AA}$  in the rest frame including the optical Fe II lines) can be well determined by the following power law function,  $f_\lambda \propto \lambda^\alpha$ . Moreover, due to the effects of the optical Fe II lines, some more complicated model should be applied to determine the AGN power law continuum, rather than to determine the continuum by the oversimplified wavelength windows (Kaspi et al. 2000, Peterson et al. 2004, Pu et al. 2006, Zhang 2013c). Due to the high noise of the spectra around the  $H\alpha$ , there are no further discussions about the red part of the spectra.

In this paper, the optical Fe II lines are modeled by the more recent Fe II template discussed in Kovacevic et al. (2010). And then, the power law function  $f_\lambda \propto \lambda^\alpha$  is applied for the AGN continuum component, and multi-gaussian functions are applied to describe the emission lines around the  $H\beta$ : two broad gaussian functions for the broad component of the  $H\beta$ , one narrow gaussian function for the narrow  $H\beta$ , two narrow gaussian functions for the  $[\text{O III}]\lambda 4959, 5007\text{\AA}$  doublet, one broad gaussian function for the  $\text{He II}\lambda 4687\text{\AA}$ . In the procedure, the main objective is to determine the AGN power law continuum, the main reason of applying two broad gaussian functions for the broad  $H\beta$  is only lead to the best fitted results for the emission lines. No further discussions are shown about the multiple components of the broad  $H\beta$ . Then, through the Levenberg-Marquardt least-squares minimization technique, the AGN power law continuum, the optical Fe II lines and the other emission lines can be well determined. Here, the best fitted results for the mean spectra rather than for all the observed spectra for each object are shown in Fig. 1. It is clear that our procedure to determine the AGN power law continuum is efficient. Finally, based on the determined power law function and the reported redshift for each QSO, the continuum luminosity at  $5100\text{\AA}$  and the corresponding spectral index can be well calculated in each epoch.

Before the end of the section, there is one point we should note. Based on the discussions in Maoz et al. (1994) and Kaspi et al. (2000), the spectrophotometric calibration has been accomplished to do the absolute flux calibration for each collected spectrum by the properties of the simultaneously observed comparison standard star. And moreover, the absolute flux calibration has an moderate uncertainty of  $\sim 10\%$ , and the relative flux calibration uncertainty is about  $\sim 3\%$ . Therefore, we do not show further discussions about the flux calibrations, but we accept that the value  $S/N \sim 10$  for the all the collected spectra, and we can clearly confirm that the relative flux calibration are accurate enough and have few effects on our determined spectra index.

### 3 OPTICAL SPECTRAL INDEX - LUMINOSITY RELATIONSHIPS FOR THE PG QSOS

Based on the well determined optical spectral indices and the AGN continuum luminosities at  $5100\text{\AA}$ , the spectral index - luminosity relationship can be tested for the 17 individual mapped PG QSOS. Before proceeding further, there is one point we should note. The following used continuum luminosity is not the directed measured value from the observed spectrum, but the value listed in the Kaspi et al. (2000) with the necessary corrections having been done for the absolute continuum flux inter-calibrations at  $5100\text{\AA}$ . Moreover, the corresponding uncertainty for the continuum flux in each epoch is the value listed in Kaspi et al. (2000).

Fig. 2 shows the optical spectral index - luminosity relationships for the 17 individual PG QSOS. The corresponding spearman rank correlation coefficient and the number of the available observed spectra are marked for each QSO in the figure. It is clear that there are no apparently strong correlations between the optical spectral index and the continuum luminosity for the mapped QSOS, besides weak trends for the relationship (coefficient still larger than -0.5 but the two-sided significance level  $p_{null}$  much smaller than 0.01) for the two PG QSOS of PG 0026 and PG 1613. Besides the direct shown optical spectral index - luminosity relationship for the 17 mapped PG QSOS, the spectra with the lowest and the highest continuum luminosities at  $5100\text{\AA}$  for each QSO are shown in Fig. 3, in order to more clearly show spectral variabilities. From the results in Fig. 2 and Fig. 3, the basic and clear results can be found that there are apparent continuum variability but the much weak corresponding spectral index variability.

Before the end of the section, two methods are applied to further check the relationships for the 17 individual QSOS: the commonly used bootstrap method to estimate the confidence levels of the coefficients and the more recent Least Trimmed Squares (LTS) robust fit method (Cappellari et al. 2013) to determine the best fitted results for the relationships.

The commonly used bootstrap method is applied as follows. Before the spearman rank correlation coefficient is calculated, the values of the optical spectral index and the continuum luminosity are re-calculated and randomly determined within the range from  $P - P_{err}$  to  $P + P_{err}$ , where  $P$  and  $P_{err}$  represent the parameter value (the optical spectral index, continuum luminosity) and the corresponding uncertainty. Then, the spearman rank coefficients are re-calculated by the new values of the optical spectral index and the continuum luminosity. The the procedure is repeated 5000 times for each QSO. The probability distributions of the re-calculated spearman rank correlation coefficients are shown in Fig. 4 for the 17 mapped PG QSOS. It is clear that even after the considerations of the parameter uncertainties, the previous results can not be changed: no apparently strong spectral index -luminosity relationship for the QSOS (the coefficient always larger than -0.5 and smaller than 0.5).

The more recent Least Trimmed Squares (LTS) robust fit method is applied to find the best fits for the correlations (Cappellari et al. 2013),  $\alpha = A + B \times \lambda L_{\lambda}$ , under the considerations of the probable intrinsic scatters of the

data points with uncertainties in both coordinates. The best fitted LTS results and the corresponding 68% and 99% confidence bands for the best fitted results are shown in Fig. 2. It is more clearer that besides the PG 0026 and PG 1613, none of the QSOS has the slope  $\alpha$  3 times larger than the corresponding uncertainty of the slope. Actually, through the LTS method, some outliers (having deviations larger than  $2.6\sigma$  from the expected relation) (solid circles in Fig 2) should be firstly ruled out, before to give the final best fitted results, which should lead to some more apparent linear fit. The outliers are perhaps due to the bad spectra quality. Meanwhile, if the outliers were also considered, the slope should be more closer to zero.

Therefore, none of the 17 QSOS have apparent optical spectral index - luminosity relationships with  $5\sigma$  confidence levels, and only two QSOS (PG 0026 and PG 0052) have probable and weak optical spectral index - luminosity relationship with  $3\sigma$  confidence levels.

### 4 DISCUSSIONS AND CONCLUSIONS

Although, there is so far no confirmed conclusion about the nature of the AGN variabilities, the more recent proposed damped random walk (DRW) model (one special stochastic model) has be well and successfully applied to describe the AGN variabilities (Bauer et al. 2009, Kelly et al. 2009, Kozłowski et al. 2010, Schmidt et al. 2010, MacLeod et al. 2010, Meusinger et al. 2011, Bailer-Jones 2012, MacLeod et al. 2012, Schmidt et al. 2012, Andrae et al. 2013, Zhang 2013b, Zu et al. 2013). The basic idea of the DRW model is that the variability  $s(t)$  has one simple exponential covariance between two different epochs  $t_i$  and  $t_j$ ,  $\langle s(t_i)s(t_j) \rangle = \sigma^2 \times \exp(-|t_i - t_j|/\tau_0)$ . Then, through the two DRW parameters, the damped intrinsic variability time scale  $\tau_0$  and the damped intrinsic variability amplitude  $\sigma$ , the AGN variabilities in both observed and unobserved epochs can be well re-produced. And moreover, the determined damped intrinsic variability time scale  $\tau_0$  can be used to understand the origination (or the principal dependent AGN parameter) of AGN variability, comparison with the theoretical characteristic time scales (Edelson & Nandra 1999). Therefore, the variability properties of the optical spectral index and the continuum emission are checked: much different (similar) damped intrinsic variability time scales should lead to weak (strong) dependence of the optical spectral index on the continuum luminosity.

Based on the well determined spectral index and the continuum emission in each epoch, the time dependent variabilities of the optical spectral index and the continuum emission for each PG QSO can be well analyzed by the well applied damped random walk method. Here, we apply the DRW method discussed in Zu et al. (2011, 2013) to describe the variabilities. In the DRW method, through the MCMC (Markov Chain Monte Carlo) analysis with the uniform logarithmic priors of the DRW parameters of  $\tau_0$  and  $\sigma$  covering every possible corner of the parameter space ( $0 < \tau_0 < 1e+5$  and  $0 < \sigma < 1e+2$ ), the posterior distributions of the DRW parameters can be well determined and provide the final accepted parameters and the corresponding statistical confidence limits. Then, based on the posterior distributions, the exponential covariance for variability is applied to produce

the corresponding variability at any epoch, i.e., the mean DRW fit and the corresponding  $1\sigma$  variance. Moreover, when the DRW method is applied, one gaussian white noise with zero mean and unit standard deviation is accepted as the model measurement noise. Fig. 5 shows the mean DRW fits for the variabilities of the optical spectral index and the continuum emission at  $5100\text{\AA}$ , and Fig. 6 shows the posterior distributions of the damped intrinsic variability time scales. Before further discussions about the damped intrinsic variability time scales, we can find that the mean DRW fits look bad for the variations of the spectral index in several cases (such as for the PG 0052 and PG 0844). We think the bad mean DRW fits are perhaps not due to the poor damped random walk parameters, but seriously due to the tiny variations of the optical spectral index and the bad time gaps. However, even the DRW parameters were poor, the shown observational variability modes in Fig. 5 could prove there are different varying modes for the spectral index and the continuum emission for the several bad cases: larger variability amplitudes for the continuum emission, but smaller amplitudes for the optical spectral index, and much different variation trends for the optical spectral index and the continuum emission.

It is clear that the varying modes are much different for the optical spectral index and for the continuum emission: the damped intrinsic variability time scales for the optical spectral index are commonly much smaller than that for the continuum emission (besides the results for PG 2130), which strongly indicates there are much different intrinsic mechanisms controlling the variabilities of the optical spectral index and the continuum emission. Thus, it can not be naturally expected for one strong dependence of the optical spectral index on the continuum luminosity. Therefore, it is clear that except the global effects of the BH masses, the host galaxy contamination, the narrow line contamination etc., no strong dependence of the optical spectral index on the continuum luminosity can be confirmed for the 17 mapped individual PG QSOs. In other words, there is no intrinsic dependence of the optical spectral index on the continuum luminosity.

Before the end of the paper, there are two points we should note. On the one hand, we should note that Pu et al. (2006) have discussed the optical spectral index - luminosity relationships for the 17 PG QSOs, and reported that most of the 17 objects show apparent correlations between the spectral slope and the continuum flux (five of them have much strong correlations with coefficients larger than 0.5), which is against our found results. The different results from Pu et al. (2006) are mainly due to the following two main reasons. The first main reason is due to the process for the continuum flux calibration, because of different instruments used for the spectra of the PG QSOs. In Pu et al. (2006), no further process is considered for the flux calibration, the values direct from the observed spectra were used. The second main reason is due to the effects of the optical Fe II lines and the probable broad He II  $\lambda 4687\text{\AA}$  line on the determined spectral slope (Bian et al. 2010, Zhang 2013c). Thus, much different results from the results in Pu et al. (2006) can be found. On the other hand, in the paper, we firstly show the direct evidence for the much different intrinsic mechanisms for the variabilities of the optical spectral index and the continuum emission by the well applied damped random walk method.

Therefore, no strong relationship between the optical spectral index and the continuum luminosity can be confirmed for the individual AGN. The much different damped intrinsic variability time scales are enough to support our final results: the common sense 'AGNs get bluer when they get brighter' is not so common.

The final conclusions are as follows.

- In order to ignore the global effects of the host stellar lights, the emission lines, the central region parameters on the relationship between the optical spectral index and the continuum luminosity, we carefully analysis the multi-epoch spectra of the well known 17 individual mapped PG QSOs in Kaspi et al. (2000), and found there is no confirmed strong dependence of the optical spectral index on the continuum luminosity, even after the considerations of the parameter uncertainties.
- The well accepted damped random walk method is applied for the variabilities of the optical spectral index and the continuum emission for the 17 PG QSOs, the damped intrinsic variability time scales are much different for the optical spectral index and the continuum emission, which strongly indicates there are much different mechanisms controlling the optical spectral index variability and the continuum emission variability.

## ACKNOWLEDGEMENTS

Z-XG very gratefully acknowledge Bailer-Jones C. A. L. in MPIA for giving us constructive comments and suggestions to greatly improve our paper. Z-XG gratefully acknowledges the kind support from the Chinese grant NSFC-11003043 and NSFC-11178003. We further gratefully thanks Dr. Kaspi S. who makes us to conveniently collect the public spectra of the 17 mapped PG QSOs (<http://wise-obs.tau.ac.il/~shai/PG/>).

## REFERENCES

- Andrae R., Kim D. W., Bailer-Jones C. A. L., 2013, *A&A*, 554, 137
- Bailer-Jones C. A. L., 2012, *A&A*, 546, A89
- Barth A. J., Nguyen M. L., Malkan M. A., Filippenko A. V., Li W. D., et al., 2011, *ApJ*, 732, 121
- Bauer A., Baltay C., Coppi P., Ellman N., Jerke J., Rabinowitz D., Scalzo R., 2009, *ApJ*, 696, 1241
- Bentz M. C., Peterson B. M., Pogge R. W., Vestergaard M., Onken C. A., 2006, *ApJ*, 644, 133
- Bentz M. C., Walsh J. L., Barth A. J., Baliber N., Bennert V. N., et al., 2009, *ApJ*, 705, 199
- Bentz M. C., Walsh J. L., Barth A. J., Yoshii Y., Woo J. H., et al., 2010, *ApJ*, 716, 993
- Bian W. H., Huang K., Hu C., Zhang L., Yuan Q. R., Huang K. L., Wang J. M., 2010, *ApJ*, 718, 460
- Breedt E., McHardy I. M., Arevalo P., et al., 2010, *MNRAS*, 403, 605
- Cappellari, M., Scott N., Alatalo K., Blitz L., Bois M., et al., 2013 *MNRAS*, 432, 1709
- Conway R. G., Kellermann K. I., Long R. J., 1963, *MNRAS*, 125, 261

- Denney K. D., Bentz M. C., Peterson B. M., Pogge R. W., Cackett E. M., et al., 2006, *ApJ*, 653, 152
- Denney K. D., Peterson B. M., Pogge R. W., Adair A., Atlee D. W., et al., 2009, *ApJL*, 704, 80
- Denney K. D., Peterson B. M., Pogge R. W., Adair A., Atlee D. W., et al., 2010, *ApJ*, 721, 715
- Edelson R. & Nandra K., 1999, *ApJ*, 514, 682
- Hawkins M. R. S. 1996, *MNRAS*, 278, 787
- Hawkins M. R. S. 2002, *MNRAS*, 329, 76
- Heeschen D. S., 1960, *PASP*, 72, 368
- Hopkins P. F., Hernquist L., Cox T. J., Di Matteo T., Robertson B., Springel V., 2006, *ApJS* 163, 1
- Kaspi S., Smith P. S., Maoz D., Netzer H., Jannuzi B. T., 1996, *ApJL*, 471, 75
- Kaspi S., Smith P. S., Netzer H., Maoz D., Jannuzi B. T., Giveon U., 2000, *ApJ*, 533, 631
- Kaspi S., Maoz D., Netzer H., Peterson B. M., Vestergaard M., Jannuzi B. T., 2005, *ApJ*, 629, 61
- Kawaguchi T., Mineshige S., Umemura M., Turner E. L. 1998, *ApJ*, 504, 671
- Kellermann K. I., Pauliny-Toth I. I. K., Williams P. J. S., 1969, *ApJ*, 157, 1
- Kelly B. C., Bechtold J., Siemiginowska A. 2009, *ApJ*, 698, 895
- Kovacevic, J., Popovic, L. C., Dimitrijevic, M. S., 2010, *ApJS*, 189, 15
- Kozłowski S., Kochanek C. S., Udalski A., Wyrzykowski L., Soszynski I., et al., 2010, *ApJ*, 708, 927
- MacLeod J. M. & Doherty L. H., 1972, *Nature*, 238, 88
- MacLeod C. L., Ivezić Z., Kochanek C. S., Kozłowski S., Kelly B., et al., 2010, *ApJ*, 721, 1014
- MacLeod C. L., Ivezić Z., Branimir S., et al., 2012, *ApJ*, 753, 106
- Maoz D., Smith P. S., Jannuzi B. T., Kaspi S., Netzer H., 1994, *ApJ*, 421, 34
- Meusinger H., Hinze A., de Hoon A., 2011, *A&A*, 525, 37
- Mushotzky R. F., Edelson R., Baumgartner W., Gandhi P., 2011, *ApJL*, 743, 12
- Peterson B. M., Ferrarese L., Gilbert K. M., Kaspi S., et al., 2004, *ApJ*, 613, 682
- Pu X., Bian W., Huang K., 2006, *MNRAS*, 372, 246
- Rees M. J. 1984, *ARA&A*, 22, 471
- Sakata Y., Minezaki T., Yoshii Y., et al., 2010, *ApJ*, 711, 461
- Schmidt K. B., Marshall P. J., Rix H. W., Jester S., Hennawi J. F., Dobler G., 2010, *ApJ*, 714, 1194
- Schmidt K. B., Rix H. W., Shields J. C., Knecht M., Hogg D. W., Maoz D., Bovy J., 2012, *ApJ*, 744, 147
- Tang S. M., Zhang S. N., Hopkins P. E., 2007, *MNRAS*, 377, 1113
- Torricelli-Ciamponi G., Foellmi C., Courvoisier T. J.-L., Paltani S. 2000, *A&A*, 358, 57
- Ulrich M. H., Maraschi L., Urry C. M., 1997, *ARA&A*, 35, 445
- Vanden Berk D. E., Wilhite B. C., Kron R. G., et al., 2004, *ApJ*, 601, 692
- Wilhite B. C., vanden Berk, D. E., Kron R. G., Schneider D. P., Pereyra N., Brunner R. J., Richards G. T., Brinkmann J. V., 2005, *ApJ*, 633, 638
- Wilhite B. C., Brunner R. J., Grier C. J., Schneider D. P., vanden Berk, D. E. 2008, *MNRAS*, 383, 1232
- Wold M., Brotherton M. S., & Shang Z. 2007, *MNRAS*, 375, 989
- Woo J. H., Treu T., Malkan M. A., Ferry M. A., Misch T., 2007, *ApJ*, 661, 60
- Zhang X. G., Dultzin D., Wang T. G., 2008, *MNRAS*, 385, 1087
- Zhang X. G., 2011, *ApJ*, 741, 104
- Zhang X. G., 2013a, *MNRAS*, 429, 2274
- Zhang X. G., 2013b, *MNRAS Letter*, 431, L112
- Zhang X. G., 2013c, *MNRAS accepted*, (arXiv:1307.0511)
- Zu Y., Kochanek C. S., Peterson B. M., 2011, *ApJ*, 735, 80
- Zu Y., Kochanek C. S., Kozłowski S., Udalski A., 2013, *ApJ*, 765, 106
- Zuo W. W., Wu X. B., Liu Y. Q., Jiao C. L., 2012, *ApJ*, 758, 104

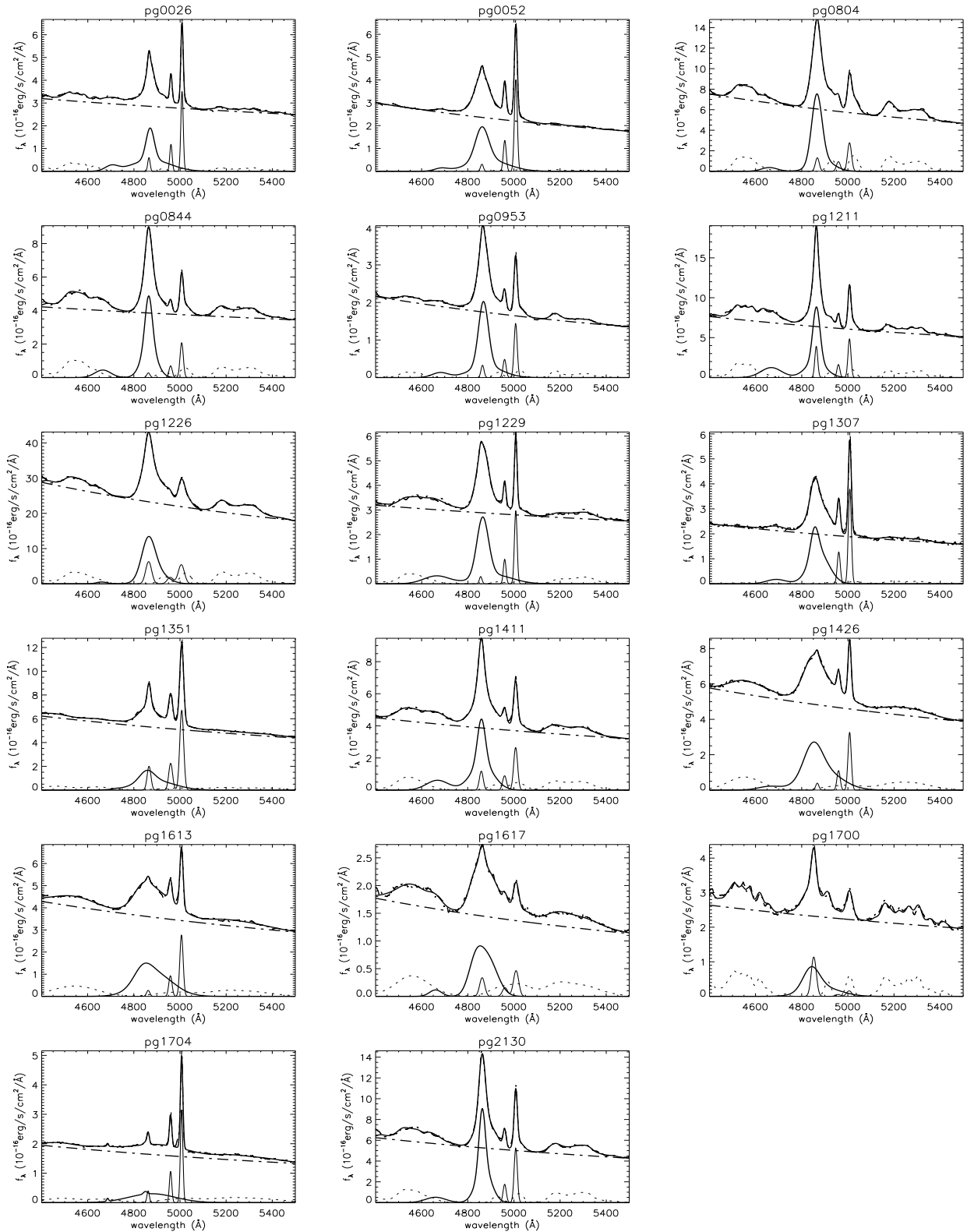


**Figure 1.** The best fitted results for the mean spectra around the  $H\beta$  of the 17 mapped PG QSOs. The thin dashed line and the thick solid line represent the observed spectrum and the corresponding best fitted result respectively. Please enlarge the figure, both the thin dashed line and the thick solid line can be clearly detected, because the observed spectrum and the best fitted result are totally overlapped. Then, the corresponding broad  $H\beta$  and probable broad  $He\ II$  line (thick solid lines), narrow lines (thin solid lines), the optical  $Fe\ II$  components (thin dotted line) and the power law continuum (thick dot-dashed line) are shown under the mean spectrum.

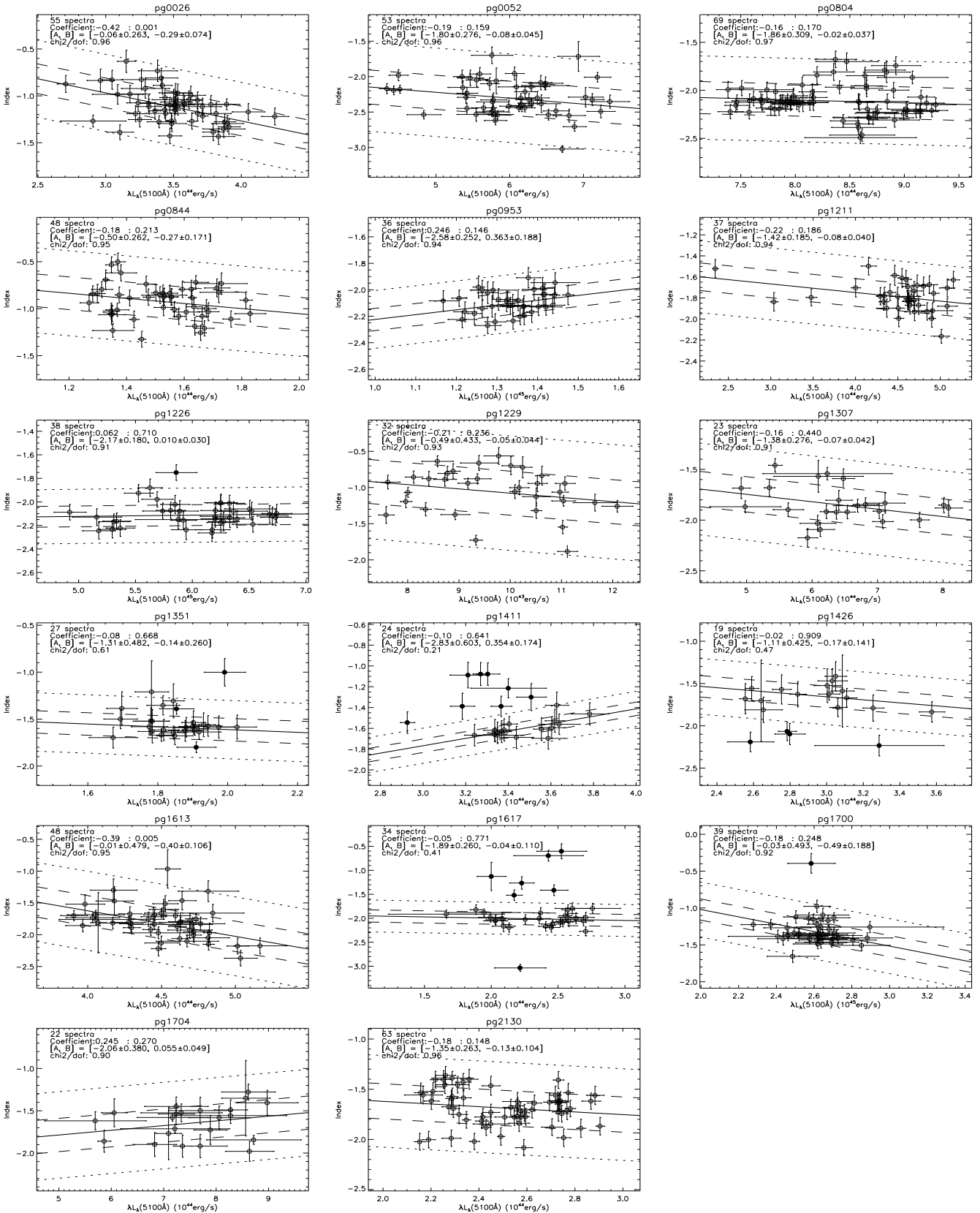


**Figure 2.** The optical spectral index - luminosity relationships for the 17 mapped PG QSOs. In the top left corner of each subfigure, the following information is shown in turn: the number of available spectra (first line), the corresponding spearman rank correlation coefficient and the parameter  $P_{null}$  (second line), the parameters  $A$  and  $B$  ( $\alpha = A + B \times \lambda_{L_x}$ ) determined by the LTS method (third line), the  $\chi^2/dof$  (fourth line) for the LTS best fitted results. In each subfigure, the solid line represents the LTS best fitted results, the dashed and dotted lines are for the corresponding 68% and 99% confidence bands for the LTS best fitted results. The solid circles are for the outliers determined by the LTS method.

© RAS, MNRAS 000, 1–??

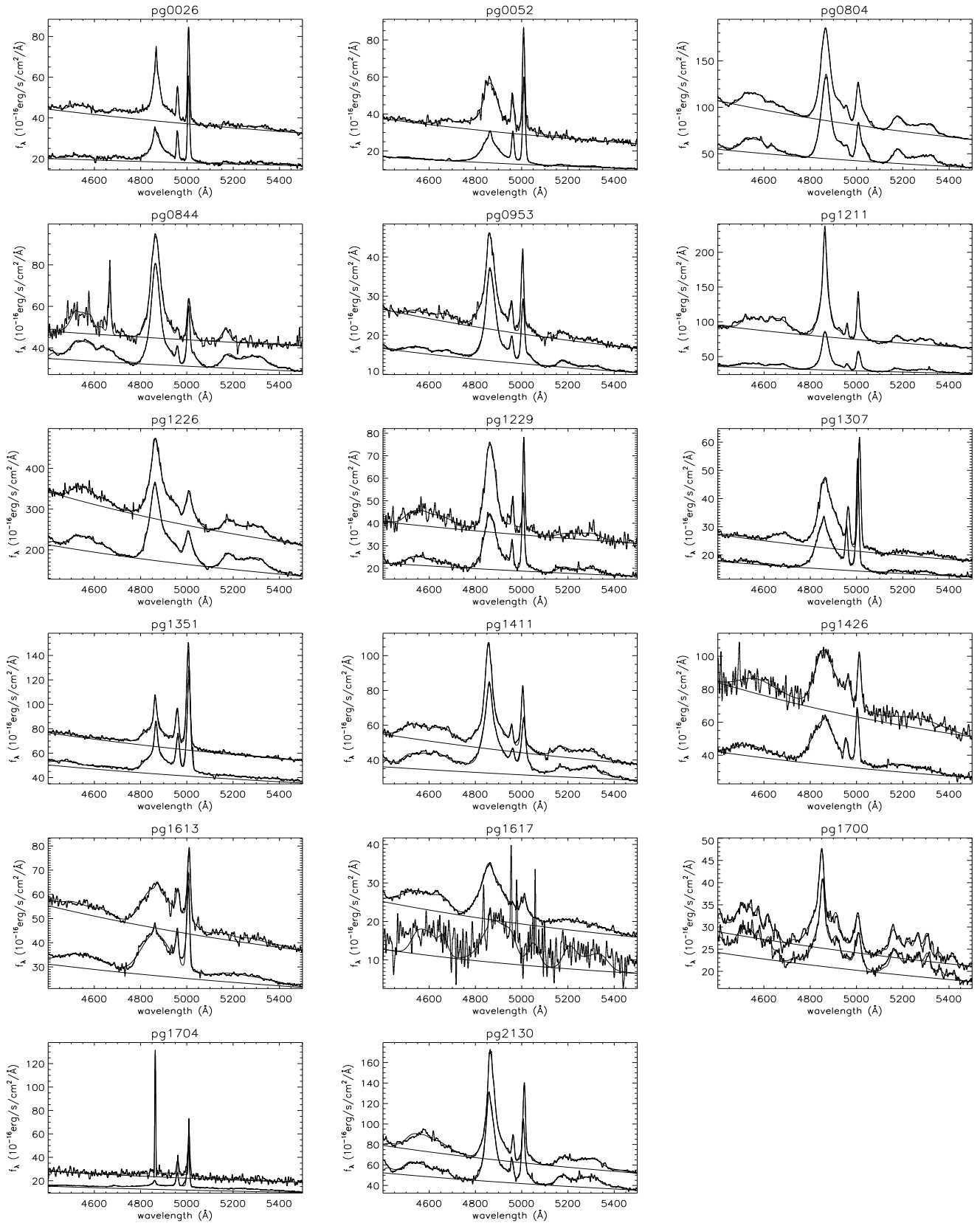


**Figure 3.** The spectra with the lowest and the highest continuum luminosity at 5100Å for each PG QSO. The thin and thick solid lines are for the observed spectrum and the corresponding best fitted result respectively. The solid line under the observed spectrum is for the determined power law AGN continuum.

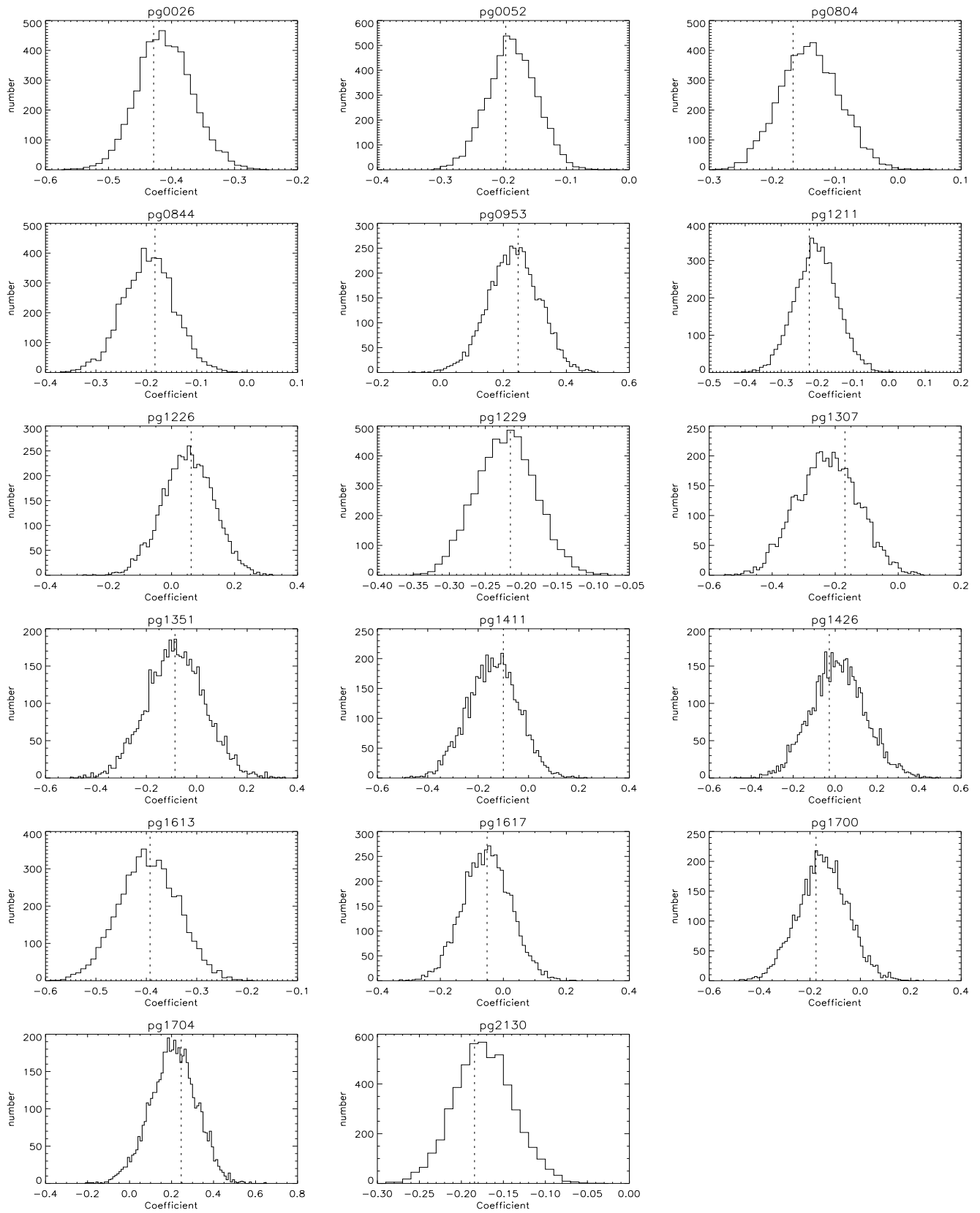


**Figure 4.** The distributions of the spearman rank correlation coefficients for the relationships between the optical spectral index and the continuum luminosity, with the considerations of the parameter uncertainties.

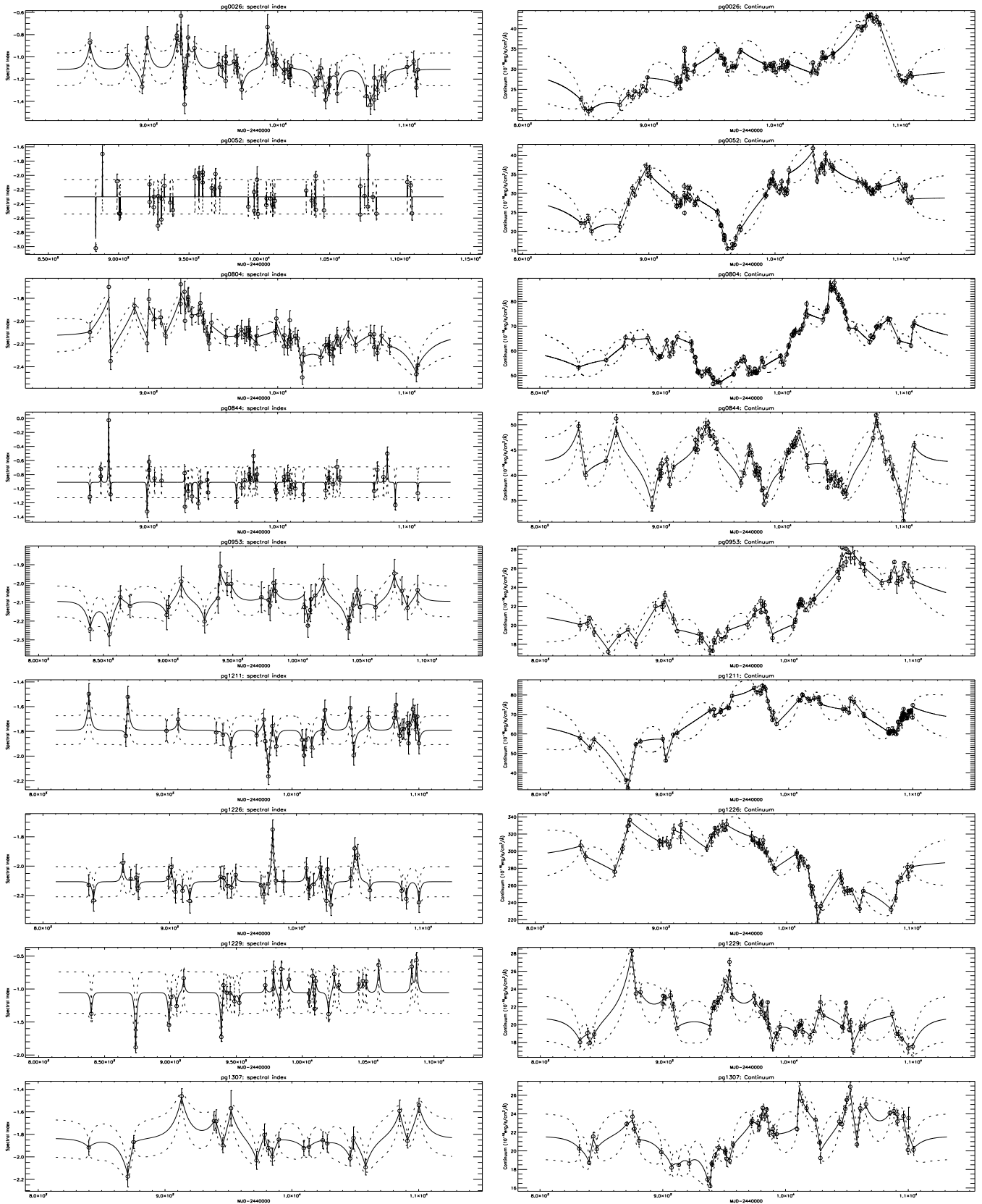


**Figure 5.** The mean DRW fits for the variabilities of the optical spectral index and the continuum emission for the 17 mapped PG QSOs by the DRW method (Zu et al. 2011, 2013) with the DRW parameters determined by the MCMC analysis. The circles are for the observational data points, the solid line and the two dotted lines are for the determined mean DRW fit and the corresponding  $1\sigma$  variance respectively. The left panels shows the results about the optical spectral index, and the right panels are for the continuum emission.

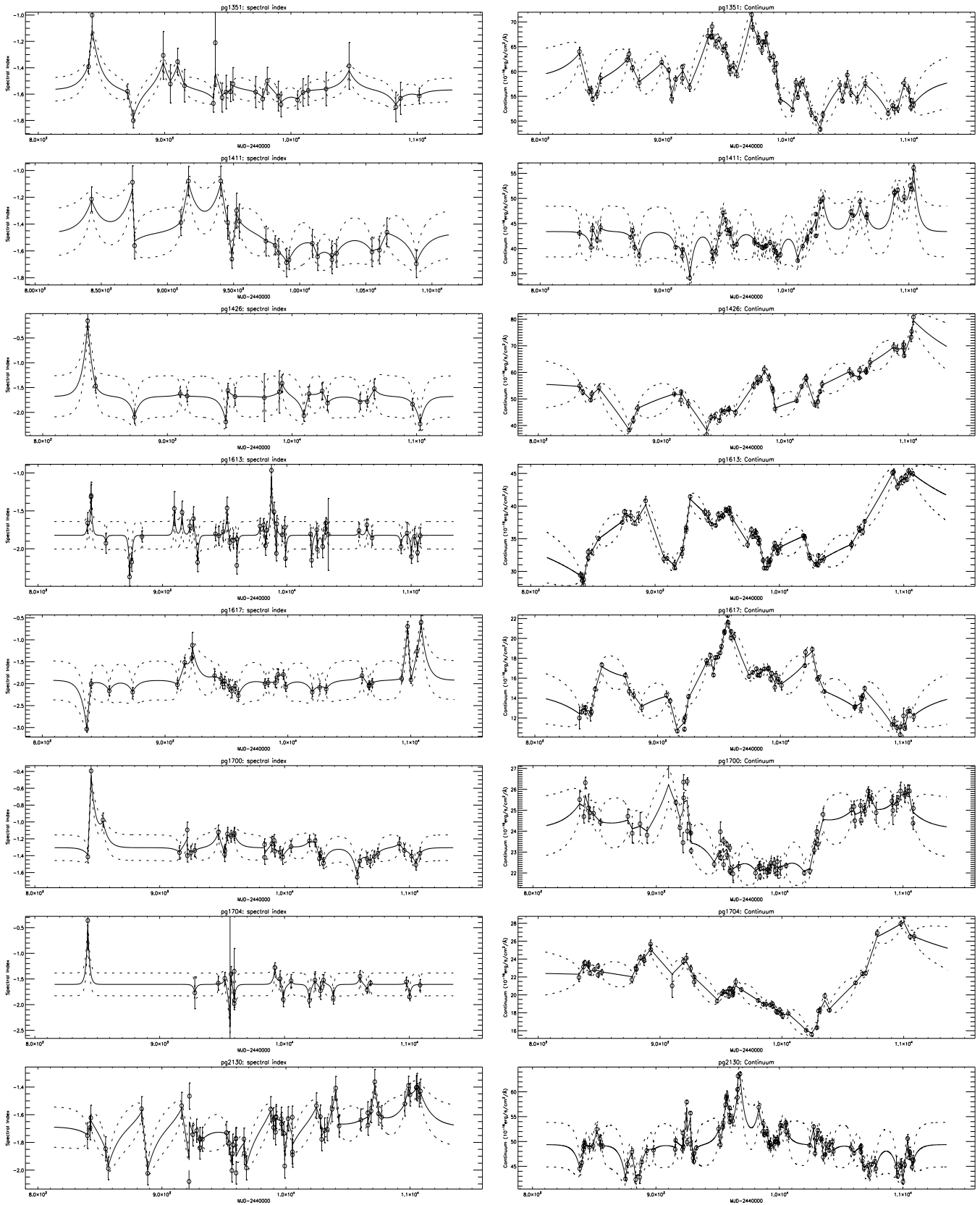
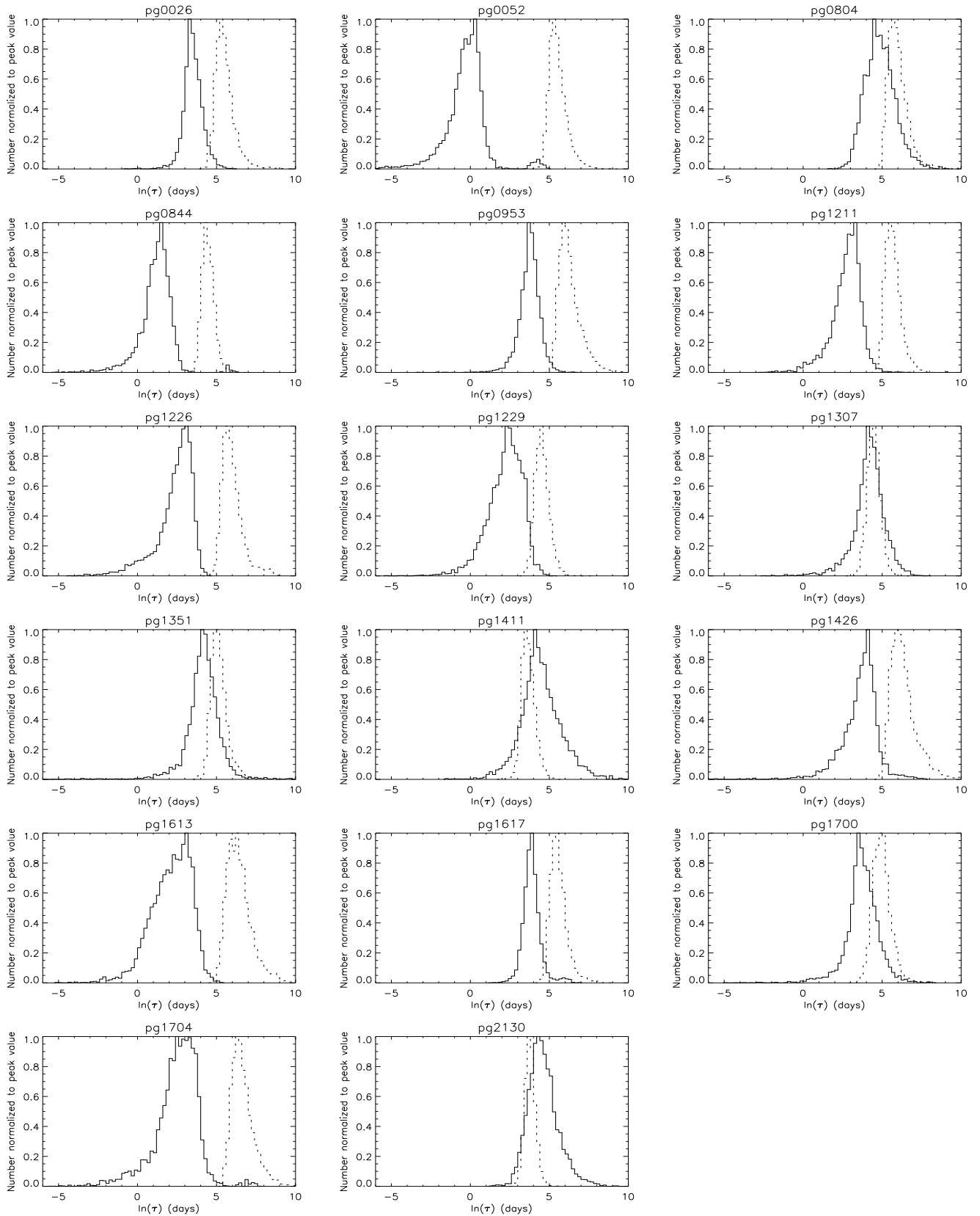


Figure 5. –Continued.



**Figure 6.** The posterior distributions of the DRW determined damped intrinsic variability time scales for the variabilities of the optical spectral index and the continuum emission, by the MCMC analysis. Solid line represents the distribution for the optical spectral index variabilities, and the dotted line is for the continuum variability.